Sliding-mode control for dc–dc converters with constant switching frequency

Y. He and F.L. Luo

Abstract: A new approach implementing the sliding-mode controller is proposed for dc–dc converters. The equivalent control input is used as the system control input, which results in a duty cycle regulation control system. As designed, equivalent control input is maintained at a value between 0 and 1, similar to the desired duty cycle value. Thus, constant switching frequency can be achieved under changes of state conditions. Two sliding-mode controllers based on this method are designed for positive output elementary Luo converter. Traditional small-signal analysis is applied to study the close-loop system performance under proposed approach. Audio-susceptibility, control-to-output transfer functions and output impedance are derived on the basis of the small-signal model. It is shown that the proposed sliding-mode control approach retains the advantages of traditional sliding-mode control, as well as achieve constant switching frequency, which is decided by the input saw-tooth waveform. Results of the experiment are reported for both controllers and they verify the theoretical analysis.

1 Introduction

The dc–dc conversion technology has been developing very rapidly, and dc–dc converters have been widely used in industrial applications such as dc motor drives, computer systems and communication equipments. Among them, positive output elementary Luo converters (POEL) [1, 2] are series dc–dc converters possessing high-voltage transfer gain and small ripple voltage and ripple current. Control for them needs to be studied for the future application of these good topologies.

Dc–dc converters are non-linear in nature. The design of high performance control for them is a challenge for both the control engineering engineers and power electronics engineers. In general, a good control for dc–dc converters always ensures stability in arbitrary operating condition. Moreover, good response in terms of rejection of load variations, input voltage changes and even parameter uncertainties is also required for a typical control scheme.

After pioneer study of dc–dc converters [3], a great deal of effort has been directed in developing the modelling and control techniques of various dc–dc converters [4, 5]. Classic linear approach relies on the state averaging techniques to obtain the state-space averaged equations [3]. From the state-space averaged model, possible perturbations are introduced into the state variables around the operating point, and small-signal state-space equations are therefore derived. On the basis of the equations, linear transfer functions of the open-loop plant can be obtained. A linear controller is easy to be designed with these necessary transfer functions based on the small-signal state-space equations. The procedure is well known [3]. However, these methods cannot ensure stability under large variations of state condition changes. They often perform unacceptably in large load and input voltage variations.

The sliding-mode control [6, 7] for variable structure systems (VSSs) is an effective non-linear approach for the control of dc–dc converters, which are VSS in nature. Various studies in the application of sliding-mode control for dc–dc converters have been reported in the past several decades [8–12]. Different sliding surfaces are proposed in those papers. All these traditional sliding-mode controllers offer several advantages for control of dc–dc converters, which includes stability under load and input voltage variations, good dynamic response and simple implementation [13]. However, a major problem exists for traditional sliding-mode control: the switching frequency of dc–dc converters under sliding-mode control is various and is determined by some state variables such as the inductor value and the hysteresis width [14].

This paper presents a new implementation method [15] to achieve a constant switching frequency sliding-mode control (CSFSMC). In detail, this method retains the advantages of traditional sliding-mode control such as ability of redefining the system trajectories, which is of first order and defined in time domain. In addition, the proposed controller has constant switching frequency. The proposed method can be summarised as below: it is known that sliding-mode control system is analysed with traditional small-signal method. The proposed approach is achieved by the concept of equivalent control input, which is of the same meaning as duty cycle input of the dc–dc converters. Thus, this equivalent control input can be used as the output of the controller. In this case, the control system looks like a traditional duty cycle control of dc–dc converters. The resultant close-loop system can retain the advantages of sliding-mode control and in addition, constant switching frequency is maintained under variations of the operation point and state conditions. The close-loop system can be analysed with small-signal method as well. The necessary transfer functions [16] such as control-to-output transfer

IEE Proceedings online no. 20050030

doi:10.1049/ip-cta:20050030

Paper first received 27th January and in revised form 19th September 2005

The authors are with the Centre for Advanced Power Electronics, School of EEE, Block S1, Nanyang Technological University, Nanyang Avenue, Singapore 639798, Singapore

E-mail: efflluo@ntu.edu.sg

function, input–output transfer function and the output impedance can be derived.

The elementary circuit of POEL is selected as an example in this paper. Two sliding surfaces are examined to derive the proposed duty cycle controllers. It can be seen that this method is widely applicable for other dc–dc converters with special design of the sliding surface. In the analysis, the instantaneous values of current and voltage are i_X and v_X for the component X. The corresponding average values are I_X and V_X. The input voltage and input current are v_{in} and i_{in}. The output voltage and output current are v_{O} and i_{O}.

2 Proposed approach: CSFSMC

The dc–dc converter bilinear state-space model can be written as

$$\dot{\boldsymbol{X}} = \boldsymbol{A}(x, t) + \boldsymbol{B}(x, t)u \tag{1}$$

where t is the time, $\boldsymbol{X} \in \Re^N$ the state vector, $\boldsymbol{A} \in \Im^N$ and $B \in \Im^N$ are state matrices, u the scalar input which often takes two values as u^+ and u^-.

The sliding surface is a combination of state variables as

$$\sigma(x, t) = \boldsymbol{GX} + \varphi = 0 \tag{2}$$

where $\boldsymbol{G}$ is a $1 \times N$ matrix as $\boldsymbol{G} = [g_1, g_2, \ldots, g_N]$ which has positive constant value. φ is some reference value calculated from the system state-space equation.

The control law of sliding-mode control is shown as

$$u = \begin{cases} u^+ & \text{for } \sigma(x, t) > 0 \\ u^- & \text{for } \sigma(x, t) < 0 \end{cases} \tag{3}$$

The system is in sliding-mode if its representing point (RP) moves on the sliding surface $\sigma(x, t) = 0$. Existence condition and reaching condition are two requirements for the stability of the sliding-mode controller.

The existence condition is represented as

$$\lim_{\sigma \to 0} \sigma \frac{\mathrm{d}\sigma}{\mathrm{d}t} < 0 \tag{4}$$

This ensures that the system RP can slide across the sliding surface.

The reaching condition means that the system RP will reach the sliding surface despite the initial position of RP in the state-space. If the system RP is in one substructure initially and the switch input is kept constant according to the sign of $\sigma(x, t)$, the system RP must be able to cross the sliding surface in finite time and the sliding function $\sigma(x, t)$ can change its sign correspondingly. This condition can be verified by checking the derivative of $\sigma(x, t)$. For example, the system RP is in the region where $\sigma(x, t) < 0$. The switch is set as $u = u^+$ according to the switching law and the system state equation is $\dot{\boldsymbol{X}} = f(x, t, u^+)$. It is then obtained

$$\frac{\mathrm{d}\sigma}{\mathrm{d}t} = \boldsymbol{G}f(x, t, u^+) + \dot{\varphi} \tag{5}$$

If $\mathrm{d}\sigma/\mathrm{d}t$ is kept at a constant positive definitive value, the system RP will cross the sliding surface eventually and the crossing time is decided by the value of $\mathrm{d}\sigma/\mathrm{d}t$.

The analysis of sliding-mode control system on sliding surface is often via the equivalent input. When on the sliding surface, the sliding function satisfies

$$\sigma(x, t) = 0 \tag{6}$$

$$\frac{\mathrm{d}\sigma}{\mathrm{d}t} = \boldsymbol{G}\dot{\boldsymbol{X}} + \dot{\varphi} = 0 \tag{7}$$

Combining (1) and (7) leads to

$$\boldsymbol{G}\dot{\boldsymbol{X}} + \dot{\varphi} = \boldsymbol{GA}(x, t) + \boldsymbol{GB}(x, t)u_{\text{eq}} + \dot{\varphi} = 0 \tag{8}$$

where the scalar control input is substituted by an equivalent control u_{eq} that represents an input of the same meaning as the duty cycle input. In conventional applications, reference part φ is some constant value calculated from the circuit parameters. The derivative of reference part φ is zero in such condition. Thus, (8) is changed to

$$\boldsymbol{G}\dot{\boldsymbol{X}} = \boldsymbol{GA}(x, t) + \boldsymbol{GB}(x, t)u_{\text{eq}} = 0 \tag{9}$$

On the assumption that $[\boldsymbol{GB}]^{-1}$ exits, one can derive the expression for the equivalent control

$$u_{\text{eq}} = -[\boldsymbol{GB}]^{-1}\boldsymbol{GA}(x, t) \tag{10}$$

Finally, by substituting (10) into (1), the close-loop system state-space equation can be achieved as

$$\dot{\boldsymbol{X}} = [\boldsymbol{I} - \boldsymbol{B}(\boldsymbol{GB})^{-1}\boldsymbol{G}]\boldsymbol{A}(x, t) \tag{11}$$

Equation (11) describes the system dynamics under sliding-mode control. However, there is another problem if one wants to use the equivalent control input as the duty cycle control. The equivalent control input represented in (10) contains no information about the reference and thus the system is not controllable with direct use of equivalent control. Thus, the reference part is proposed to be substituted with function of reference voltage with order higher than 1, which makes its derivative still contain reference information. In addition, the derivative of φ should be zero in steady state to satisfy (9). In this paper, the integral of the error between the output voltage and the reference voltage is recommended. Therefore the proposed sliding surface is described as

$$\sigma(x, t) = \boldsymbol{GX} + \int_0^t (v_{\text{O}} - V_{\text{r}})\,\mathrm{d}t \tag{12}$$

In such case, the derivative of φ contains the information of reference voltage and it is zero in steady state, which also satisfies (9). The equivalent control changes to

$$u_{\text{eq}} = -[\boldsymbol{GB}]^{-1}[\boldsymbol{GA}(x, t) + (v_{\text{O}} - V_{\text{r}})] \tag{13}$$

Because this control scheme uses the equivalent control as the duty cycle input to the converter circuit, the converter performance is the same as the open-loop circuit in the steady state. Therefore the switching frequency can be selected using the open-loop model according to the requirements of ripple voltage and current. Once the switching frequency is chosen, the cross-over frequency of the low-pass filter could be defined. The general control scheme for this proposed approach is shown in Fig. 1.

The components of coefficients matrix $\boldsymbol{G}$ need not be all non-zero numbers. It has been proved that part state information is enough for achieving satisfactory control result [12]. In the next section, the sliding surfaces which contain one and two state variables are examined with the proposed approach.

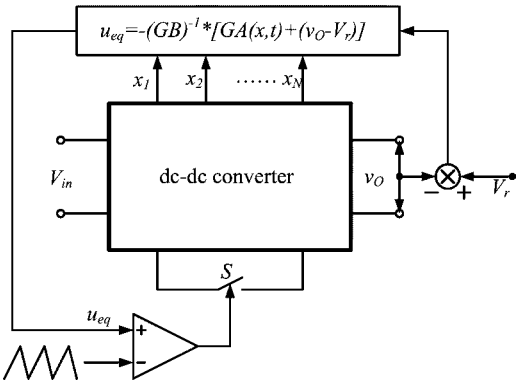

Fig. 1 *General control scheme of the CSFSMC*

3 CSFSMC for POEL converter

3.1 Model of POEL converter

Fig. 2 shows the topology of POEL converter. The equivalent circuits of POEL converter under switch on are shown in Fig. 3*a*, and Fig. 3*b* shows the equivalent circuits under switch off. This paper does not consider the circuit works in discontinuous conduction mode.

The state vector includes four components as: inductor current i_{L_1}, capacitor voltage v_{C_1}, inductor current i_{L_2} and the output voltage v_O. The state vector is shown as

$$\boldsymbol{X} = [i_{L_1} \quad v_{C_1} \quad i_{L_1} \quad v_O]^T \tag{14}$$

With equivalent circuits shown in Fig. 3, one can derive the system open-loop state-space equation as

$$\dot{\boldsymbol{X}} = \boldsymbol{A}(x, t) + \boldsymbol{B}(x, t)u \tag{15}$$

where

$$\boldsymbol{A}(x,t) = \begin{bmatrix} -\dfrac{1}{L_1}x_2 \\ \dfrac{1}{C_1}x_1 \\ -\dfrac{1}{L_2}x_4 \\ \dfrac{1}{C_2}x_3 - \dfrac{1}{RC_2}x_4 \end{bmatrix} \quad \text{and}$$

$$\boldsymbol{B}(x,t) = \begin{bmatrix} \dfrac{1}{L_1}(x_2 + v_{in}) \\ -\dfrac{1}{C_1}(x_1 + x_3) \\ \dfrac{1}{L_2}(x_2 + v_{in}) \\ 0 \end{bmatrix}$$

This equation also gives the steady-state information of POEL converter if the discrete scalar input u is considered

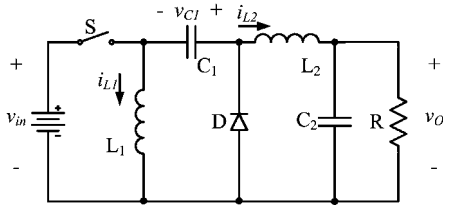

Fig. 2 *Topology of POEL converter*

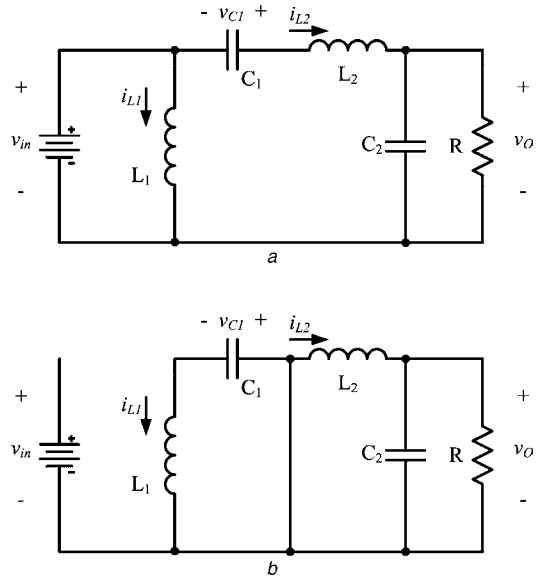

Fig. 3 *Equivalent circuits of POEL converter during switch on and off*

a Switch on
b Switch off

as a continuous duty cycle input. If the operating point is selected as $u = K$ $(0 < K < 1)$, the operating point of the state vector could be derived as

$$\boldsymbol{X} = \left[\frac{K^2 v_{in}}{R(1-K)^2} \quad \frac{K v_{in}}{(1-K)} \quad \frac{K v_{in}}{R(1-K)} \quad \frac{K v_{in}}{(1-K)}\right]^T \tag{16}$$

$u = 1$ means the switch S is ON all the time, the system reaches a stable state which is represented as

$$\boldsymbol{X} = [\infty \quad -V_{in} \quad 0 \quad 0]^T \tag{17}$$

$u = 0$ means the switch S is OFF all the time, another system stable state is obtained as

$$\boldsymbol{X} = [0 \quad 0 \quad 0 \quad 0]^T \tag{18}$$

If the switching frequency is f and the duty cycle is k, the ripple of input inductor current i_{L_1} is [2]

$$\Delta i_{L_1} = \frac{kV_{in}}{fL_1} \tag{19}$$

The ripple of output voltage is [2]:

$$\Delta v_O = \frac{kV_{in}}{16f^2 C_2 L_2} \tag{20}$$

3.2 Sliding surface with one state variable

The state variable can be chosen as the input inductor current or output voltage for control of dc–dc converters. For POEL converter, existence condition is not satisfied for the sliding surface with only output voltage feedback. The input inductor current is chosen in this paper. Therefore

$$\boldsymbol{G}_1 = [g_{11} \quad 0 \quad 0 \quad 0] \tag{21}$$

The sliding surface is

$$\sigma(x, t) = g_{11}x_1 + \int_0^t (v_O - V_r)\,dt = 0 \tag{22}$$

To study the stability of the controller, discrete switch law is first chosen as

$$u = \begin{cases} 0 & \text{when } \sigma(x,t) > 0 \\ 1 & \text{when } \sigma(x,t) < 0 \end{cases} \tag{23}$$

The existence condition is represented as

$$\lim_{\sigma\to 0^-} \frac{\mathrm{d}\sigma}{\mathrm{d}t} = \lim_{\sigma\to 0^-} \left\{ \frac{g_{11}}{L_1} v_{\text{in}} + (x_4 - V_{\text{r}}) \right\} > 0 \tag{24}$$

$$\lim_{\sigma\to 0^+} \frac{\mathrm{d}\sigma}{\mathrm{d}t} = \lim_{\sigma\to 0^+} \left\{ -\frac{g_{11}}{L_1} x_2 + (x_4 - V_{\text{r}}) \right\} < 0 \tag{25}$$

Because it is in the vicinity of the sliding surface, it is reasonable to say that $x_4 - V_{\text{r}}$ is very small. v_{in} and x_2 are positive. Therefore a large value of g_{11}/L_1 can satisfy the existence condition.

The reaching condition is verified as follows. If system RP is in a region where $\sigma(x, t)$ is negative, on the assumption that system RP cannot reach the sliding surface, then the switch should be kept on. The system RP will converge to a point represented in (17). Correspondingly, the derivative of $\sigma(x,t)$ can be calculated as

$$\lim_{t\to\infty} \left.\frac{\mathrm{d}\sigma}{\mathrm{d}t}\right|_{\sigma<0} = \frac{g_{11}}{L_1} v_{\text{in}} - V_{\text{r}} \tag{26}$$

It can be seen that if g_{11} is selected properly, (26) can be a positive constant value. Thus, $\sigma(x,t)$ will increase and system RP will reach the sliding surface sooner or later. If the system RP is in a region where $\sigma(x, t)$ is positive, the proof is similar and the equation can be written as

$$\lim_{t\to\infty} \left.\frac{\mathrm{d}\sigma}{\mathrm{d}t}\right|_{\sigma>0} = -V_{\text{r}} \tag{27}$$

V_{r} is a positive constant, (27) is therefore satisfied. The system RP will reach the sliding surface in finite time. In summary, the requirements of $\boldsymbol{G}$ to satisfy the two conditions is that

$$g_{11} > \frac{L_1 V_{\text{r}}}{v_{\text{in}}} \tag{28}$$

The equivalent control input can be calculated using (13), (15) and (21). It is shown as

$$u_{\text{eq}} = \frac{g_{11}x_2 - L_1(x_4 - V_{\text{r}})}{g_{11}(V_{\text{in}} + x_2)} \tag{29}$$

In this paper, equivalent control will be used as the control input compared with a saw-tooth waveform. A constant switching frequency pulse-waveform is thus generated to control the switch.

By substituting (29) into (15), the close-loop system on the sliding surface can be obtained as

$$\frac{\mathrm{d}}{\mathrm{d}t}\boldsymbol{X} = \begin{cases} -\dfrac{1}{g_{11}} x_4 + \dfrac{1}{g_{11}} V_{\text{r}} \\ \dfrac{1}{C_1} x_1 - \dfrac{(x_1 + x_3)(g_{11}x_2 - L_1(x_4 - V_{\text{r}}))}{g_{11}C_1(V_{\text{in}} + x_2)} \\ \dfrac{1}{L_2} x_2 - \dfrac{1}{L_2} x_4 - \dfrac{L_1}{g_{11}L_2}(x_4 - V_{\text{r}}) \\ \dfrac{1}{C_2} x_3 - \dfrac{1}{RC_2}\, x_4 \end{cases} \tag{30}$$

It is a non-linear equation. Setting the left side of (30) equal to zero, it is found that this equation has only one equilibrium point as

$$\boldsymbol{X}_{\text{eq}} = \begin{bmatrix} \dfrac{V_{\text{r}}^2}{V_{\text{in}}R} & V_{\text{r}} & \dfrac{V_{\text{r}}}{R} & V_{\text{r}} \end{bmatrix}^{\text{T}}$$

By introducing the perturbation around the operating point as

$$\begin{cases} \boldsymbol{X} = \boldsymbol{X}_{\text{op}} + \Delta\boldsymbol{X} \\ v_{\text{r}} = V_{\text{r}} + \Delta v_{\text{r}} \\ v_{\text{in}} = V_{\text{in}} + \Delta v_{\text{in}} \end{cases} \tag{31}$$

The small-signal state-space equation is derived as

$$\frac{\mathrm{d}}{\mathrm{d}t}\boldsymbol{X} = \boldsymbol{A}_{S_1}\Delta\boldsymbol{X} + \boldsymbol{B}_{S_1}\Delta v_{\text{r}} + \boldsymbol{E}_{S_1}\Delta v_{\text{in}} + \boldsymbol{F}_{S_1}\Delta i_{\text{O}} \tag{32}$$

where

$$\boldsymbol{A}_{S_1} = \begin{bmatrix} 0 & 0 & 0 & -\dfrac{1}{g_{11}} \\ \dfrac{V_{\text{in}}}{C_1(V_{\text{r}} + V_{\text{in}})} & \dfrac{-V_{\text{r}}}{C_1R(V_{\text{in}} + V_{\text{r}})} & \dfrac{-V_{\text{r}}}{C_1(V_{\text{r}} + V_{\text{in}})} & \dfrac{L_1V_{\text{r}}}{g_{11}RC_1V_{\text{in}}} \\ 0 & \dfrac{1}{L_2} & 0 & -\dfrac{g_{11} + L_1}{g_{11}L_2} \\ 0 & 0 & \dfrac{1}{C_2} & -\dfrac{1}{RC_2} \end{bmatrix}$$

$$\boldsymbol{B}_{S_1} = \begin{bmatrix} \dfrac{1}{g_{11}} & \dfrac{L_1V_{\text{r}}}{g_{11}RC_1V_{\text{in}}} & \dfrac{L_1}{g_{11}L_2} & 0 \end{bmatrix}^{\text{T}}$$

$$\boldsymbol{E}_{S_1} = \begin{bmatrix} 0 & -\dfrac{V_{\text{r}}^2}{RC_1V_{\text{in}}(V_{\text{in}} + V_{\text{r}})} & 0 & 0 \end{bmatrix}^{\text{T}}$$

$$\boldsymbol{F}_{S_1} = \begin{bmatrix} 0 & 0 & 0 & -\dfrac{1}{C_2} \end{bmatrix}^{\text{T}}$$

The system stability and dynamic properties can be examined from (32). If all the poles of matrix $\boldsymbol{A}_S$ are in the left plane, the close-loop system is stable on the sliding surface. $\boldsymbol{G}$ should be selected according to (28) and also to achieve satisfactory system dynamic response. System stability because of the parameter uncertainties can be studied by varying the parameters in the matrix $\boldsymbol{A}_{S_1}$ and examining its corresponding poles.

The input-to-output transfer function $\boldsymbol{G}_{\text{vin}}(s)$ and reference-to-output transfer function $\boldsymbol{G}_{\text{vref}}(s)$ of the system could be derived from (30) as

$$\begin{cases} \boldsymbol{G}_{\text{vin}}(s) = [0 \quad 0 \quad 0 \quad 1] * (s * \boldsymbol{I} - \boldsymbol{A}_{S_1})^{-1} * \boldsymbol{B}_{S_1} \\ \boldsymbol{G}_{\text{vref}}(s) = [0 \quad 0 \quad 0 \quad 1] * (s * \boldsymbol{I} - \boldsymbol{A}_{S_1})^{-1} * \boldsymbol{W}_{S_1} \end{cases} \tag{33}$$

Output impedance is defined as [16]

$$Z_{\text{out}}(s) = \frac{v_{\text{O}}(s)}{i_{\text{O}}(s)} \tag{34}$$

These three transfer functions can be derived. Given the specified value for circuit and controller parameters, these transfer functions can be easily computed with the help of Matlab. They will be useful for choosing the controller parameters. For length of paper, the representations of these

transfer functions are not shown in the paper. The design principle for choosing $\boldsymbol{G}$ is to achieve a stable system with fast response in tracking reference voltage, and keeping $\boldsymbol{G}_{\text{vin}}(s)$ and $Z_{\text{out}}(s)$ in a low level over large frequency range. Because the equivalent control is based on the averaged model which is valid in low frequency, the sensed variables should first be filtered to remove the high frequency part. Low-pass filters with cross-over frequency equal to a quarter of the switching frequency can be used. The resultant close-loop control scheme of controller 1 is shown in Fig. 4.

3.3 Sliding surface with two state variables

In fact, there are many possible combinations for selecting two state variables for a fourth order POEL converter. In this paper, the sliding surface with the input inductor current and the output voltage is chosen. Therefore the coefficients matrix is

$$\boldsymbol{G}_2 = [g_{21} \quad 0 \quad 0 \quad g_{24}] \tag{35}$$

And the resultant sliding surface is

$$\sigma(x, t) = g_{21}x_1 + g_{24}x_4 + \int_0^t (v_{\text{O}} - V_{\text{r}})\,\mathrm{d}t = 0 \tag{36}$$

The discrete switch law is the same as controller 1. The existence condition is changed to

$$\lim_{\sigma\to 0^-}\frac{\mathrm{d}\sigma}{\mathrm{d}t} = \lim_{\sigma\to 0^-}\left\{\frac{g_{21}}{L_1}v_{\text{in}} + \frac{g_{24}}{C_2}\left(x_3 - \frac{x_4}{R}\right) + (x_4 - V_{\text{r}})\right\} > 0 \tag{37}$$

$$\lim_{\sigma\to 0^+}\frac{\mathrm{d}\sigma}{\mathrm{d}t} = \lim_{\sigma\to 0^+}\left\{-\frac{g_{11}}{L_1}x_2 + \frac{g_{24}}{C_2}\left(x_3 - \frac{x_4}{R}\right) + (x_4 - V_{\text{r}})\right\} < 0 \tag{38}$$

The newly added part $(x_3 - (x_4/R))$ in (37) and (38) is just the value of capacitive current i_{C_2}. Thus, it is replaced by i_{C_2} in the following part of this paper. i_{C_2} is small value in the vicinity of the sliding surface. Thus, (37) and (38) can be satisfied with the same consideration as controller 1.

The reaching condition is verified with the same method as controller 1. The resultant requirements for the selection of coefficients matrix are

$$g_{21} > \frac{L_1 V_{\text{r}}}{v_{\text{in}}} \tag{39}$$

The equivalent control can be calculated by combining (13), (15) and (35). It is shown as

$$u_{\text{eq}} = \frac{g_{21}C_2x_2 - g_{24}L_1 i_{C_2} - L_1C_2(x_4 - V_{\text{r}})}{g_{21}C_2(V_{\text{in}} + x_2)} \tag{40}$$

Substituting (40) into (15), one can derive the close-loop system equation under controller 2 as

$$\frac{\mathrm{d}}{\mathrm{d}t}\boldsymbol{X} = \begin{cases} -\dfrac{g_{24}}{g_{21}C_2}\left(x_3 - \dfrac{x_4}{R}\right) - \dfrac{1}{g_{21}}x_4 + \dfrac{1}{g_{21}}V_{\text{r}} \\ (x_1 + x_3)(g_{21}C_2x_2 - L_1 g_{24}(x_3 - (x_4/R)) \\ \dfrac{1}{C_1}x_1 - \dfrac{-L_1C_2(x_4 - V_{\text{r}}))}{g_{21}C_1C_2(V_{\text{in}} + x_2)} \\ \dfrac{1}{L_2}x_2 - \dfrac{1}{L_2}x_4 - \dfrac{L_1 g_{24}(x_3 - (x_4/R))}{g_{21}C_2L_2} - \dfrac{L_1}{g_{21}L_2}(x_4 - V_{\text{r}}) \\ \dfrac{1}{C_2}x_3 - \dfrac{1}{RC_2}x_4 \end{cases} \tag{41}$$

Equation (41) has only one equilibrium point similar to the one of (30). By introducing perturbations same as (31), the small-signal state-space equation of (41) is derived as

$$\frac{\mathrm{d}}{\mathrm{d}t}\boldsymbol{X} = \boldsymbol{A}_{S_2}\Delta\boldsymbol{X} + \boldsymbol{B}_{S_2}\Delta v_{\text{r}} + \boldsymbol{E}_{S_2}\Delta v_{\text{in}} + \boldsymbol{F}_{S_2}\Delta i_{\text{O}} \tag{42}$$

where

$$\boldsymbol{A}_{S_2} = \begin{bmatrix} 0 & 0 & -\dfrac{g_{24}}{g_{21}C_2} & \dfrac{g_{24} - C_2}{g_{21}C_2} \\ \dfrac{V_{\text{in}}}{C_1(V_{\text{r}} + V_{\text{in}})} & \dfrac{-V_{\text{r}}}{C_1R(V_{\text{in}} + V_{\text{r}})} & \dfrac{-V_{\text{r}}}{C_1(V_{\text{r}} + V_{\text{in}})} + \dfrac{g_{24}L_1V_{\text{r}}}{g_{21}C_1C_2V_{\text{in}}R} & \dfrac{-g_{24}L_1V_{\text{r}}}{g_{21}C_1C_2V_{\text{in}}R^2} + \dfrac{L_1V_r}{g_{21}C_1V_{\text{in}}R} \\ 0 & \dfrac{1}{L_2} & \dfrac{-L_1 g_{24}}{L_2C_2 g_{21}} & -\dfrac{g_{21} + L_1}{g_{21}L_2} + \dfrac{L_1 g_{24}}{g_{21}RL_2C_2} \\ 0 & 0 & \dfrac{1}{C_2} & -\dfrac{1}{RC_2} \end{bmatrix}$$

$$\boldsymbol{B}_{S_2} = \begin{bmatrix} \dfrac{1}{g_{21}} & \dfrac{L_1V_{\text{r}}}{g_{21}RC_1V_{\text{in}}} & \dfrac{L_1}{g_{11}L_2} & 0 \end{bmatrix}^{\text{T}}$$

$$\boldsymbol{E}_{S_2} = \begin{bmatrix} 0 & -\dfrac{V_{\text{r}}^2}{RC_1V_{\text{in}}(V_{\text{in}} + V_{\text{r}})} & 0 & 0 \end{bmatrix}^{\text{T}}$$

$$\boldsymbol{F}_{S_2} = \begin{bmatrix} \dfrac{g_{24}}{g_{21}C_2} & \dfrac{L_1 g_{24}V_{\text{r}}}{g_{21}RC_1C_2V_{\text{in}}} & \dfrac{L_1 g_{24}}{g_{21}C_2L_2} & -\dfrac{1}{C_2} \end{bmatrix}^{\text{T}}$$

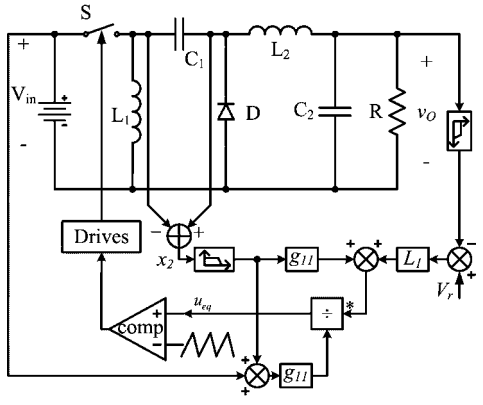

Fig. 4 *Close-loop control scheme for controller 1*

The transfer functions required for designing the controller can be derived with the same method as for controller 1. They are not shown in this paper.

The resultant close-loop control scheme for controller 2 is shown in Fig. 5. It should be noted that the capacitor current i_{C_2} also needs to be filtered before possible use in calculating the equivalent control input.

4 Design example

In the design example, the parameters for POEL converter are chosen as follows: $V_{in} = 12$ V, $C_1 = 47$ μF, $C_2 = 100$ μF, $L_1 = L_2 = 1$ mH, $R = 22\ \Omega$ and $V_r = 8$ V. The switching frequency is chosen as 20 kHz. The cross-over frequency of the low-pass filter is selected as 5 kHz, which permits a fast enough response speed of the close-loop control system and removes the ripple components effectively.

The controller design criterion is to maintain a stable and fast dynamic response, low overshoot in the reference voltage tracking and low overshoot of input inductor current. It is also necessary to achieve a low output impedance and audio-susceptibility over a wide bandwidth.

For controller 1, there is only one freedom in choosing the parameters. g_{11} should be first chosen to satisfy (28). Knowing the circuit parameters shown earlier, (28) can be solved to be

$$g_{11} > 0.00067 \tag{43}$$

Considering that most dc–dc converters are required to work in a large range of operating point, the value of g_{11} should be chosen to be larger than the value calculated from (43). Next, various value of g_{11} can be tested by examining its influence on the close-loop system performance. Fig. 6 shows the bode plot of reference-to-output transfer function $\boldsymbol{G}_{1\text{ref}}(s)$ under conditions when g_{11} is equal to 0.001, 0.005 and 0.01, respectively. It can be seen that the cross-over frequency of $\boldsymbol{G}_{1\text{ref}}(s)$ decreases when g_{11} increases, this means the system response time is longer. If this transfer function is treated as second order, the quality factor will increase when g_{11} increases, which causes the overshoot in reference tracking to increase. Thus, to obtain a trade-off in the response speed and overshoot in output voltage, the controller parameter is selected as

$$\boldsymbol{G}_1 = [g_{11} \quad 0 \quad 0 \quad 0] = [0.005 \quad 0 \quad 0 \quad 0] \tag{44}$$

For controller 2, the reaching condition requirement is the same as for controller 1, which means $g_{21} > 0.00067$ in the

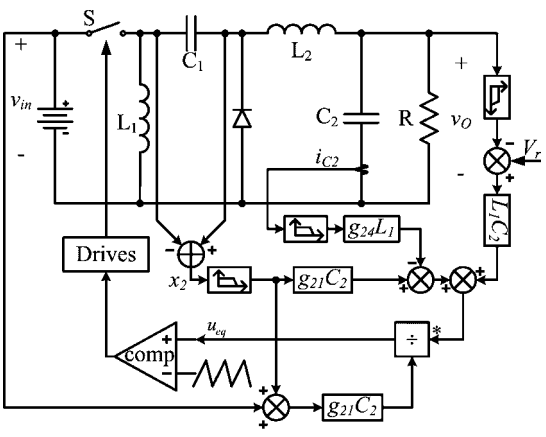

Fig. 5 *Close-loop control scheme for controller 2*

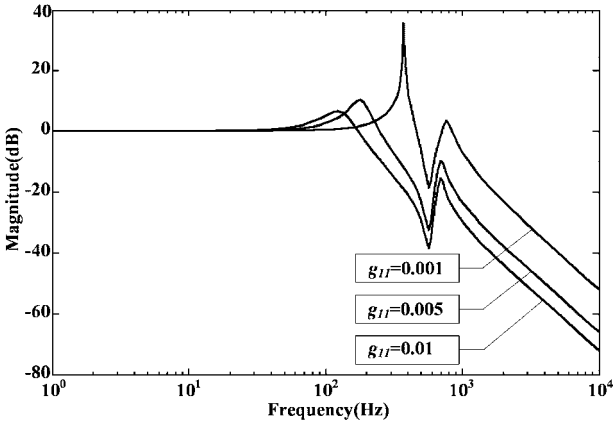

Fig. 6 *Bode plot of the reference-to-output transfer function for controller 1 with various* $\boldsymbol{G}_1$

above given circuit condition. However, unlike controller 1, controller 2 has two parameters to be chosen. Thus, it is possible to achieve a fast response by keeping the quality factor in a low level, that is a low overshoot in output voltage tracking. Fig. 7 shows the bode plot of $\boldsymbol{G}_{2\text{ref}}(s)$ under various value of controller parameters. Owing to the previous considerations, it is then chosen

$$\boldsymbol{G}_2 = [g_{21} \quad 0 \quad 0 \quad g_{24}] = [0.005 \quad 0 \quad 0 \quad 0.0005] \tag{45}$$

From Figs. 6 and 7, it can be seen that controller 2 has a quality factor smaller than that of controller 1 in the condition of same band-width, which means introducing the output voltage into the sliding surface makes the close-loop system response with lower overshoot.

With the chosen parameters for two controllers, it is also required to check whether audio-susceptibility and output impedance are kept in a low level. Fig. 8 shows audio-susceptibility of the open-loop circuit and also those of the two close-loop system. The output impedance of the open-loop circuit and two close-loop control systems are shown in Fig. 9. It can be seen that controller 2 is better than controller 1 in all close-loop characteristics.

It should be noted that the new implementation method of sliding-mode control does not change the system performance. Sliding surfaces 1 and 2, with traditional sliding-mode control implementation method, can all be thought as a kind of current-mode control. Therefore they all will increase the system output impedance in low frequency range [16]. However, the maximum value in $Z_{\text{out}}(s)$ is

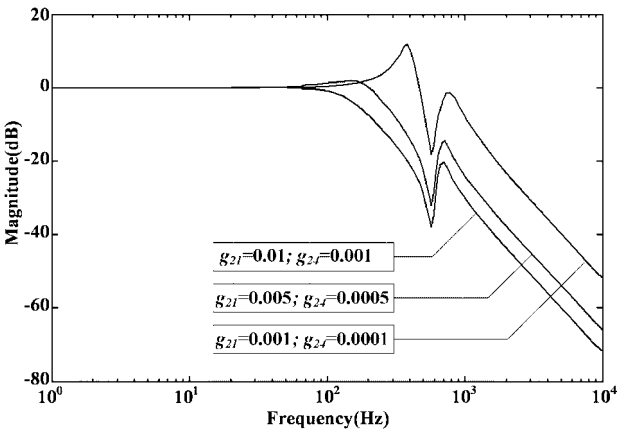

Fig. 7 *Bode plot of the reference-to-output transfer function for controller 2 with various* $\boldsymbol{G}_2$

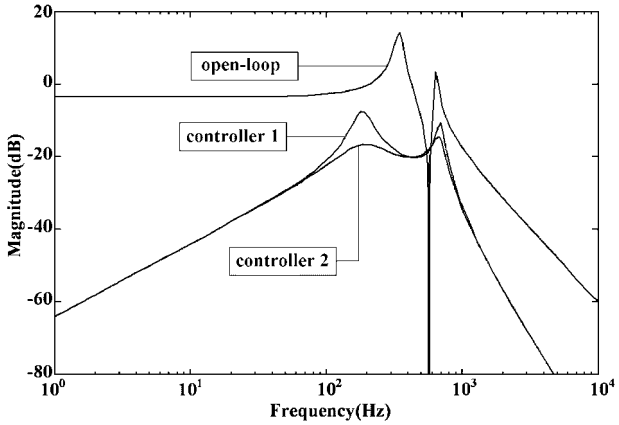

Fig. 8 *POEL converter's audio-susceptibility under various conditions*

decreased from 26.8 to 21.6 dB Ω for controller 1, and from 26.8 to 17.8 dB Ω for controller 2.

5 Simulation and experiment results

The performances of both controllers are compared with a traditional current-mode multi-loop controller [16] with PI regulator in the voltage loop for generation of current reference. This controller is also known as current-mode PI controller. In the current loop of the system, hysteresis control is used to keep a switching frequency of 20 kHz at nominal operating condition. In order to allow comparison, the closed-loop band width of the current-mode PI controller is also set to be about the same as the two proposed controllers.

Simulations are done with PSim [17] and the simulation step is set at 1 μs for three systems. Figs. 10–12 show the behaviours of output voltage and input inductor current for all three controllers in the case of reference voltage step changes from 0 to 8 V as start up performance, and then, the reference voltage is changed from 8 to 18 V at 20 ms and from 18 to 8 V at 40 ms. In particular:

1. Fig. 10 shows the system response with current-mode PI control. During start up, the input inductor current increases too fast and the overshoot is about 310% when compared with its nominal value in steady state, which is necessary for a fast voltage regulation with about 10 ms settling time. The output voltage overshoot is ∼2 V. When the reference voltage changes to 18 V, the response is similar. When reference voltage changes down to 8 V, the response is slower because of the discharge time for the output capacitor C_2 and the overshoot of output voltage is large.
2. Fig. 11 shows the system response with controller 1. It is seen that both current and voltage overshoot are higher. In addition, the settling time is longer during increase of reference voltage. When reference voltage changes down to 8 V, the response is better than the current-mode PI controller, smaller overshoot and shorter settling time are observed.
3. Fig. 12 shows the system response with controller 2. During start up, the output voltage overshoot is <0.5 V when compared with 2 V for the current-mode PI controller. At the same time, the current overshoot is decreased from 310% of current-mode PI controller to 130%. Similarly, when reference voltage increase to 18 V, again, output voltage and input inductor current increases fast and with smaller overshoot to the desired value. It is similar to the performance of controller 1 when the reference voltage decreases to 8 V and also better than the current-mode PI controller.

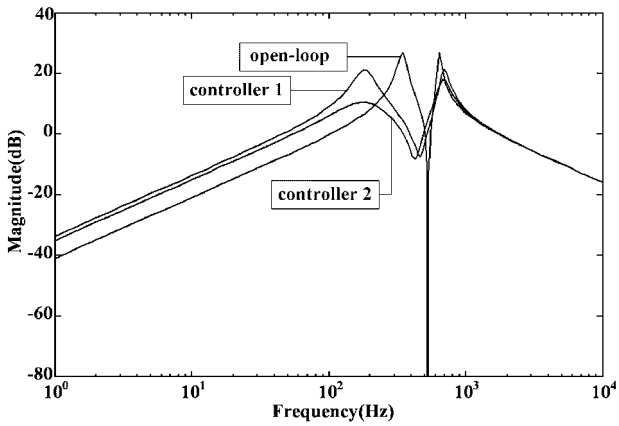

Fig. 9 *POEL converter's output impedance under various conditions*

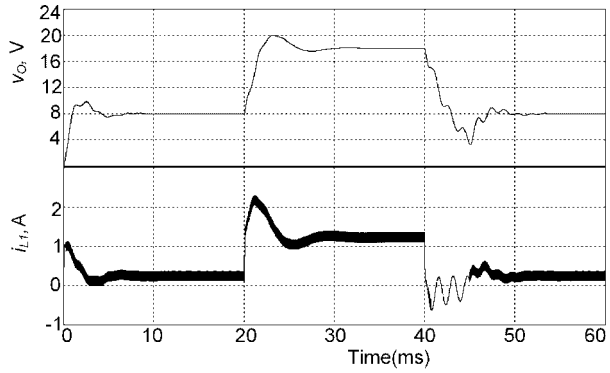

Fig. 10 *Current-mode PI controller's performance under step changes of reference voltage*

In summary, controller 2 has the best overall performance. It is evident that proposed implementation method keeps the advantages of sliding-mode control. The start up response can be shaped in the time domain. In addition, as it is actually implemented with duty cycle control, the switching frequency is strictly kept constant by the input of the saw-tooth waveform.

Both controllers for POEL converter are implemented in the experiments to show their performance predicted by the theoretical analysis and simulation results. During the experiments, all voltage waveforms are captured with AC coupling. The system conditions are the same as those mentioned in Section 4. To approximate the ideal condition as much as possible, the switch is using a TOSHIBA 2SK2267 MOSFET, and its $R_{ds\text{-}ON}$ is only

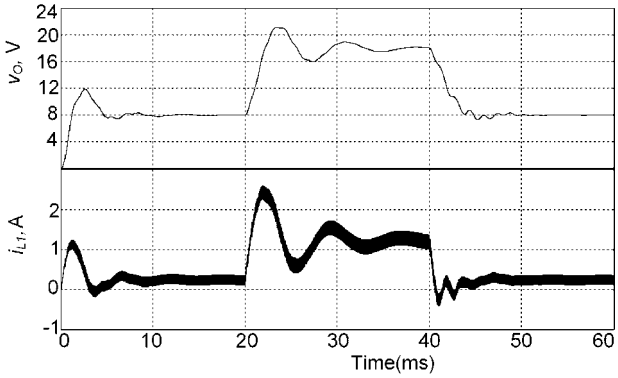

Fig. 11 *Controller 1's performance under step changes of reference voltage*

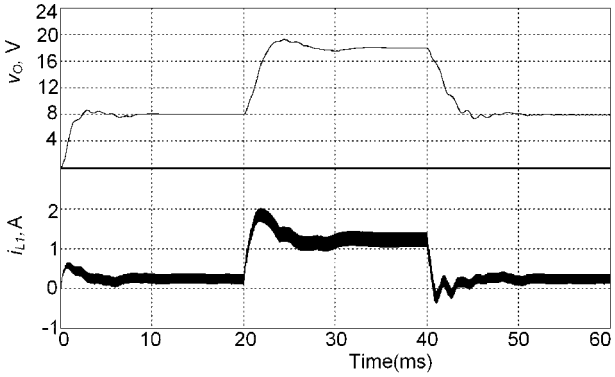

Fig. 12 *Controller 2's performance under step changes of reference voltage*

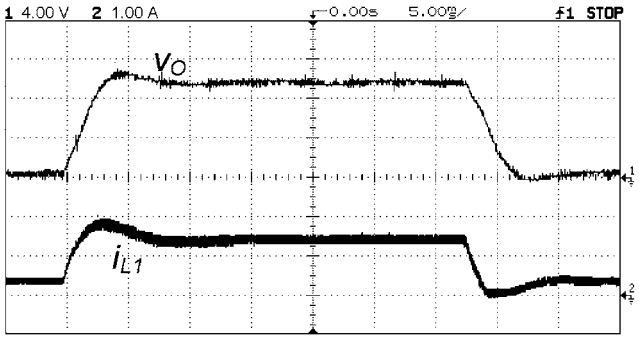

Fig. 15 *The output voltage and input inductor current waveforms for step change of reference voltage with controller 2: ch1 v_O and ch2 i_{L_1}*

8 mΩ. Low voltage drop diodes, with type MBR6045WT of MOTOROLA Company, are used in the experiments. The saw-tooth waveform is generated by the IC chip ICL8038, and the switching frequency is set as 20 kHz. The comparator is realised with IC chip LM319. In addition, inductors with small resistance are used. Parameters of controller 1 and controller 2 are chosen as shown in (44) and (45). And thus, the steady-state error is very small in each experiment.

Figs. 13 and 14 show the dynamic response of the system with controller 1 under step change of reference voltage from 8 to 18 V. Figs. 15 and 16 show the dynamic response of the system with controller 2 under the same condition. Controller 2 exhibits a faster response with lower overshoot than controller 1, which verifies the comparative results of the reference-to-output transfer functions for both controllers. With the equivalent control input waveforms shown in Figs. 14 and 16, it can be seen that the constant switching frequency is achieved with this proposed implementation method, the equivalent control input converges to a constant value equal to the desired duty cycle.

Fig. 17 shows the controller 1's performance during step change of load resistance from 22 to 11 Ω and recovers. The voltage drop is small, which is less than 2 V. The overshoot in current is almost none. Fig. 18 shows the controller 1's response to a step change of input voltage from 12 to 18 V and recovers. Because the controller has an input voltage feed-forward, the system only exhibits a small variations in the output voltage.

Fig. 19 shows the controller 2's performance during step change of load resistance from 22 to 11 Ω and recovers. Fig. 20 shows the controller 2's response to a step change of input voltage from 12 to 18 V and recovers. Both responses are similar to controller 1, which can be predicted from the system transfer functions shown in Figs. 8 and 9.

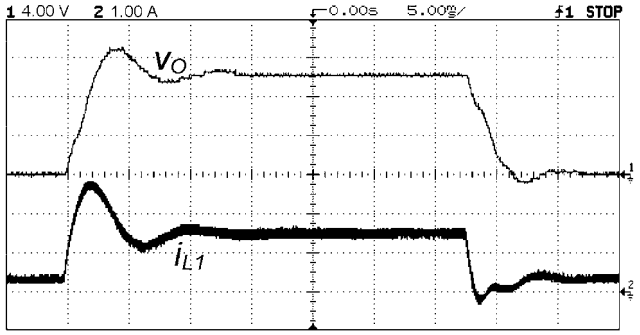

Fig. 13 *Output voltage and input inductor current waveforms for step change of reference voltage with controller 1: ch1 v_O and ch2 i_{L_1}*

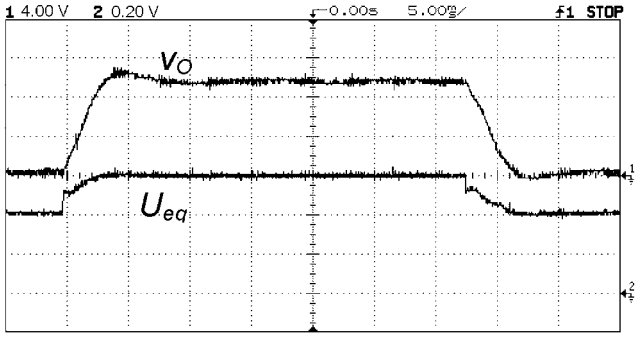

Fig. 16 *Output voltage and input inductor current waveforms for step change of reference voltage with controller 2: ch1 v_O and ch2 u_{eq}*

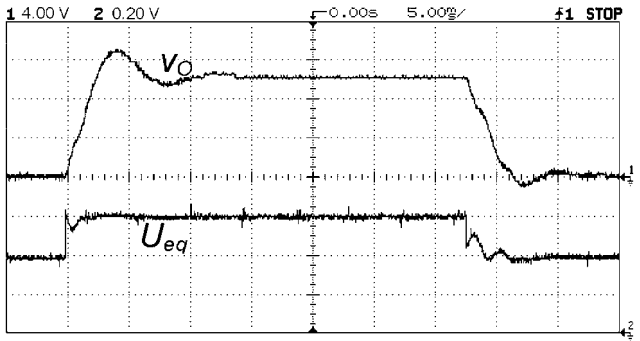

Fig. 14 *Output voltage and equivalent control waveforms under step change of reference voltage with controller 1: ch1 v_O and ch2 u_{eq}*

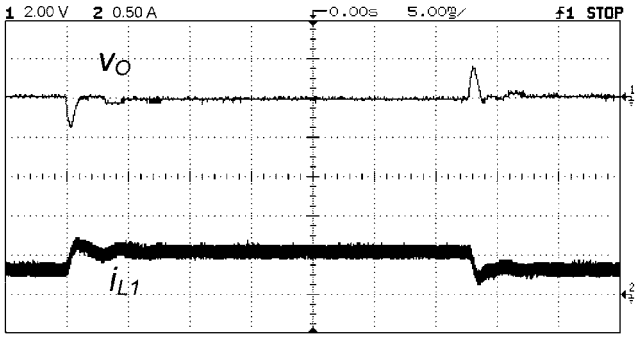

Fig. 17 *Output voltage and input inductor current waveforms for step change of load resistance with controller 1: ch1 v_O and ch2 i_{L_1}*

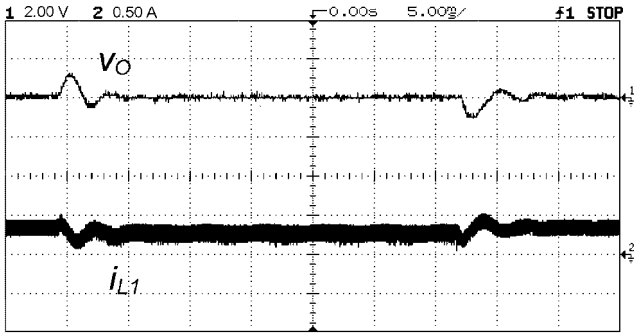

Fig. 18 *Output voltage and input inductor current waveforms for step change of input voltage with controller 1: ch1 v_O and ch2 i_{L_1}*

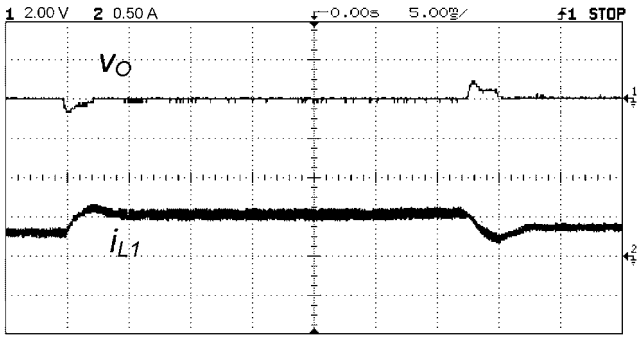

Fig. 19 *Output voltage and input inductor current waveforms for step change of load resistance with controller 2: ch1 v_O and ch2 i_{L_1}*

Because the equivalent control is calculated under ideal condition, the switching loss and other power losses in the converter are not considered in the computation. Thus, in practical, the output voltage of the system with CSFSMC may have steady-state error; the output voltage will be smaller than the reference value. In addition, the proposed controller also has steady-state error when facing system condition changes. The problem may be verified through Figs. 14–17. This problem can be solved by adding another sliding-mode controller, which will not only influence the switching frequency but, however, enhances the system performance quite well. This point will be reported in another technical paper.

6 Conclusions

A new implementation method, CSFSMC, for sliding-mode control was proposed. An integral item is added into the normal sliding surface to incorporate the new approach. One current-mode sliding surface and a two-variable sliding surface were examined with the proposed approach.

It is shown that the proposed approach design procedure is the same as a traditional sliding-mode control. The resultant controller also has the advantages possessed by the traditional sliding-mode control. The close-loop system trajectories is decided by the sliding-mode controller and not belonging to the system characteristics. In addition, the proposed approach can achieve a constant switching frequency, which is difficult for conventional approach.

Various transfer functions for the proposed close-loop control systems are derived to prove the excellent characteristics. Simulation and experiment results were also given to verify the theoretical analysis. POEL converter is selected as an example in the paper. It has been proved that this

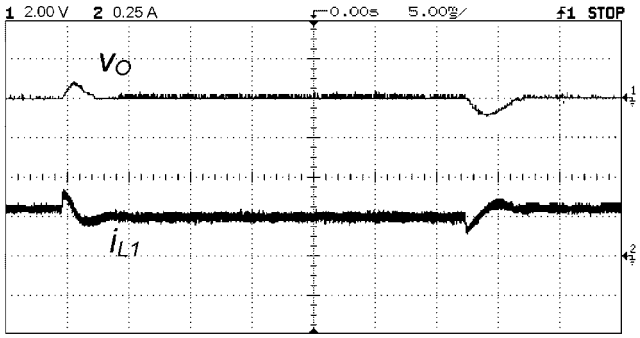

Fig. 20 *Output voltage and input inductor current waveforms for step change of input voltage with controller 2: ch1 v_O and ch2 i_{L_1}*

novel concept of implementing sliding-mode control attractive points in dc–dc converter applications. This proposed approach is also widely applicable to other dc–dc converters.

To make this proposed approach also applicable for un-ideal conditions, the power loss item should be included in the controller. This is the future work and will be addressed out in future papers.

7 References

1 Luo, F.L.: 'Positive output Luo converters: voltage lift technique', *IEE – EPA*, 1999, **146**, (4), pp. 415–432
2 Luo, F.L., and Ye, H.: 'Advanced DC/DC converters' (CRC Press, Boca Raton, USA, 2004)
3 Middlebrook, R.D., and Cuk, S.: 'Advances in switched-mode power conversion: Volumes I and II' (TESLAco, Pasadena, California, 1983)
4 Sanders, S.R., Verghese, G.C., and Cameron, D.E.: 'Nonlinear control of switching power converters', *Control Theory Adv. Technol.*, 1989, **5**, (4), pp. 601–627
5 Liu, Y.F., and Sen, P.C.: 'A general unified large signal model of current programmed DC-to-DC converters', *IEEE Trans. Power Electron.*, 1994, **9**, (4), pp. 414–424
6 Uktin, V.I.: 'Sliding modes and their application in variable structure systems' (MIR Publishers, Moscow, Russia, 1978)
7 Itkis, U.: 'Control systems of variable structure' (John Wiley & Sons, New York, USA, 1976)
8 Venkataramanan, R., Savanovic, A., and Cuk, S.: 'Sliding mode control of DC-to-DC converters'. Proc. IECON' 1985, pp. 251–258, 1985
9 Sira-Ramirez, H.: 'Sliding motions in bilinear switched networks', *IEEE Trans. Circuits Syst.*, 1987, **34**, (8), pp. 919–933
10 Sira-Ramirez, H., Ortega, R., Perez-Moreno, R., and Garcia-Esteban, M.: 'A sliding mode controller-observer for DC-to-DC power converters: a passivity approach'. Proc. 34th IEEE Conf. Decision and Control, 13–15 December 1995, Vol. 4, pp. 3379–3384
11 Mahdavi, J., Emadi, A., and Toliyat, H.A.: 'Application of state space averaging method to sliding mode control of PWM DC/DC converters'. Proc. IEEE Ind. Appl. Soc. Ann. Meeting, 5–9 October 1997, pp. 820–827
12 Oppenheimer, M., Husain, I., Elbuluk, M., and De Abreu-Garcia, J.A.: 'Sliding mode control of the cuk converter'. Proc. IEEE Power Electronics Specialists Conf., PESC '96 Record, 27th Annual IEEE, Vol. 2, 23–27 June 1996, pp. 1519–1526
13 Skvarenina, T.L.: 'The power electronic handbook' (CRC Press, Boca Raton, USA, 2002)
14 Caedoso, B.J., Moreira, A.F., Menezes, B.R., and Cortizo, P.C.: 'Analysis of switching frequency reduction methods applied to sliding mode controlled DC–DC converters'. Proc. APEC '92, 23–27 February 1992, pp. 403–410
15 He, Y., and Luo, F.L.: 'Analysis of Luo convertors with voltage-lift circuit'. *IEE Proc. Electr. Power Appl.*, **152**, (5), September 2005, pp. 1239–1252
16 Erickson, R.W., and Makismovic, D.: 'Fundamentals of power electronics' (Kluwer Academic Publishers, USA, 2001, 2nd edn.)
17 PSim version 4.1, Powersim Solutions, Inc., 585 Grove St, Suite 130, Herndon VA, 20170 USA, sales@powersimsolutions.com